PERGAMON

Planetary and Space Science 49 (2001) 1467–1479

Planetary and Space Science

www.elsevier.com/locate/planspasci

The MESSENGER mission to Mercury: scientific payload

Robert E. Gold[a,*], Sean C. Solomon[b], Ralph L. McNutt Jr.[a], Andrew G. Santo[a], James B. Abshire[c], Mario H. Acuña[c], Robert S. Afzal[c], Brian J. Anderson[a], G. Bruce Andrews[a], Peter D. Bedini[d], John Cain[d], Andrew F. Cheng[a], Larry G. Evans[c], William C. Feldman[e], Ronald B. Follas[c], George Gloeckler[d,f], John O. Goldsten[a], S. Edward Hawkins III[a], Noam R. Izenberg[a], Stephen E. Jaskulek[a], Eleanor A. Ketchum[c], Mark R. Lankton[g], David A. Lohr[a], Barry H. Mauk[a], William E. McClintock[g], Scott L. Murchie[a], Charles E. Schlemm II[a], David E. Smith[c], Richard D. Starr[c], Thomas H. Zurbuchen[d]

[a] *The John Hopkins University Applied Physics Laboratory, Laurel, MD 20723, USA*
[b] *Department of Terrestrial Magnetism, Carnegie Institution of Washington, Washington, DC 20015, USA*
[c] *NASA Goddard Space Flight Center, Greenbelt, MD 20771, USA*
[d] *Department of Atmospheric, Oceanic, and Space Sciences, University of Michigan, Ann Arbor, MI 48109, USA*
[e] *Los Alamos National Laboratory, Los Alamos, NM 87545, USA*
[f] *Department of Physics, University of Maryland, College Park, MD 20742, USA*
[g] *Laboratory for Atmospheric and Space Physics, University of Colorado, Boulder, CO 80303, USA*

Received 1 November 2000; accepted 12 January 2001

Abstract

The MErcury, Surface, Space ENvironment, GEochemistry, and Ranging (MESSENGER) mission will send the first spacecraft to orbit the planet Mercury. A miniaturized set of seven instruments, along with the spacecraft telecommunications system, provide the means of achieving the scientific objectives that motivate the mission. The payload includes a combined wide- and narrow-angle imaging system; γ-ray, neutron, and X-ray spectrometers for remote geochemical sensing; a vector magnetometer; a laser altimeter; a combined ultraviolet-visible and visible-infrared spectrometer to detect atmospheric species and map mineralogical absorption features; and an energetic particle and plasma spectrometer to characterize ionized species in the magnetosphere.

1. Introduction

Mercury, the least studied of the terrestrial planets, holds the prospect for unraveling important aspects of the origin and early history of the solar system (Solomon et al., 2001). Mercury is a challenging body to orbit, however, because of high propulsive-energy requirements and the severe thermal environment (Santo et al., 2001). To date, Mercury has been visited by spacecraft only during the three flybys by Mariner 10 in 1974 and 1975 (e.g., Dunne and Burgess, 1978; Chapman, 1988). The MErcury, Surface, Space ENvironment, GEochemistry, and Ranging (MESSENGER) spacecraft will be the first to visit Mercury in more than 30 years and the first spacecraft ever to enter Mercury orbit.

Launched in March 2004, MESSENGER will orbit Mercury for one Earth year following two flybys of Venus and two of Mercury (Santo et al., 2001). The MESSENGER mission has been designed on the basis of a detailed progression from the science questions to be answered, through mission design and implementation (Solomon et al., 2001), to the instrument suite needed to obtain the necessary data. By adhering strictly to the science requirements while also pursuing aggressively miniaturization and packaging optimization so as to minimize payload mass, we have fielded an instrument set that meets all mission constraints while enabling the measurements required for addressing fully the science questions that define the mission. The flowdown from science objectives to measurement requirements for

* Corresponding author. Tel.: +1-240-228-5412; fax: +1-240-228-6556.
E-mail address: rob.gold@jhuapl.edu (R.E. Gold).

0032-0633/01/$ - see front matter
PII: S0032-0633(01)00086-1

MESSENGER is described in the companion paper by Solomon et al. (2001).

2. Instrument suite

MESSENGER carries seven scientific instruments. Together with the spacecraft telecommunications system, these instruments provide the full set of measurements required by the MESSENGER scientific objectives (Solomon et al., 2001). The selected instruments accomplish the required observations at low cost with the low masses essential for implementing this difficult mission. Mass restrictions on a Mercury mission are severe. The total mass available for the payload, including all electronics, thermal accommodations, booms, brackets, and cables, is about 40 kg.

The instrument suite includes the Mercury Dual Imaging System (MDIS), a Gamma-Ray and Neutron Spectrometer (GRNS), an X-Ray Spectrometer (XRS), a Magnetometer (MAG), the Mercury Laser Altimeter (MLA), the Mercury Atmospheric and Surface Composition Spectrometer (MASCS), an Energetic Particle and Plasma Spectrometer (EPPS), and Radio Science (RS). MDIS has both a wide-angle (WA) and a narrow-angle (NA) imager. MASCS includes an Ultraviolet-Visible Spectrometer (UVVS) and a Visible-Infrared Spectrograph (VIRS). EPPS includes an Energetic Particle Spectrometer (EPS) sensor and a Fast Imaging Plasma Spectrometer (FIPS). Basic characteristics of each element of the payload, including its mass, power, and data rate, are listed in Table 1.

The MESSENGER instruments capitalize on emerging technologies developed over several years at The Johns Hopkins University Applied Physics Laboratory (JHU/APL), the NASA Goddard Space Flight Center (GSFC), the University of Colorado Laboratory for Atmospheric and Space Physics (LASP), and the University of Michigan. Instrument development for MDIS, GRNS, XRS, and EPPS is the responsibility JHU/APL. Responsibility of development of MLA resides at the GSFC, that for MASCS at LASP, and that for the FIPS head of EPPS at the University of Michigan. MAG is a shared development between GSFC and JHU/APL.

All instruments except MAG are fixed and body mounted for high reliability and low cost. The directional instruments are all co-aligned and located on the bottom deck of the spacecraft. Despite the extreme thermal inputs at Mercury, aperture heat-rejection filtering is required only for MDIS and MLA, since the internal spacecraft thermal environment is benign by design (Santo et al., 2001).

Redundant, compact, shared Data Processing Units (DPUs) and instrument power systems include high-level electronics, power converters, power switching, and data processing and compression for instruments to reduce mass and power. In addition, several instruments have a miniature processing unit to perform their real-time, event-by-event processing. Because of the limited downlink bandwidth available to MESSENGER, data compression is vital for this mission. Several lossless and lossy data compression techniques are provided as central services to all instruments as required.

Table 1
MESSENGER scientific payload

	Mass (kg)	Power (W)	Data rate[a]
MDIS			
Dual imagers, 1024 × 1024			
Narrow: 1.5° FOV, b&w	2.0	10.0	381 b/s,
Wide: 10.5° FOV, 12-filter wheel	2.5		32.9 Mb/d
Scanning mirror and controls	1.0		
GRNS			122 b/s,
CsI γ-ray + Li n^0 spectrometer	9.0	4.5	10.6 Mb/d
XRS			49 b/s,
X-ray spectrometer, 1–10 keV	4.0	8.0	4.2 Mb/d
MAG			
Fluxgate magnetometer	1.5	2.0	14.2 b/s,
3.6-m boom	2.0		1.2 Mb/d
MLA			46.3 b/s,
Laser altimeter, 1000-km range	5.0	20.0	4.0 Mb/d
MASCS			
UV/Visible spectrometer	1.5	1.5	86.9 b/s,
Visible/IR spectrograph	1.0	1.5	7.5 Mb/d
EPPS			
Energetic particle spectrometer			140 b/s,
Fast imaging plasma spectrometer	2.25	2.0	12.1 Mb/d
RS			
X-band transponder			
DPU	5.0	18.0	10 b/s,
Integrated electronics, power processing for all instruments			0.86 Mb/d
Instrument harness, brackets, and attachments	3.25		
Payload totals[b]	40.0	67.5	73.4 Mb/d

[a]Data rates are mission averages for the orbit phase in bits per second.
[b]Spacecraft housekeeping and attitude adds 5.0 Mb/d for a total of 78.4 Mb/d.

3. Mercury Dual Imaging System (MDIS)

MDIS meets all of the imaging requirements (Solomon et al., 2001) by combining a 12-filter (two "clear" plus 10 colors) WA imager with a high-resolution, NA imager into a single unit. The layout of MDIS is shown in Fig. 1, and its key characteristics are listed in Table 2. An internal scan mirror in MDIS provides for full coverage of the planet during orbital operations and during the two Mercury flybys. The common scan mirror and dichroic heat-rejection filter keep the imagers compact. The MDIS charge-coupled

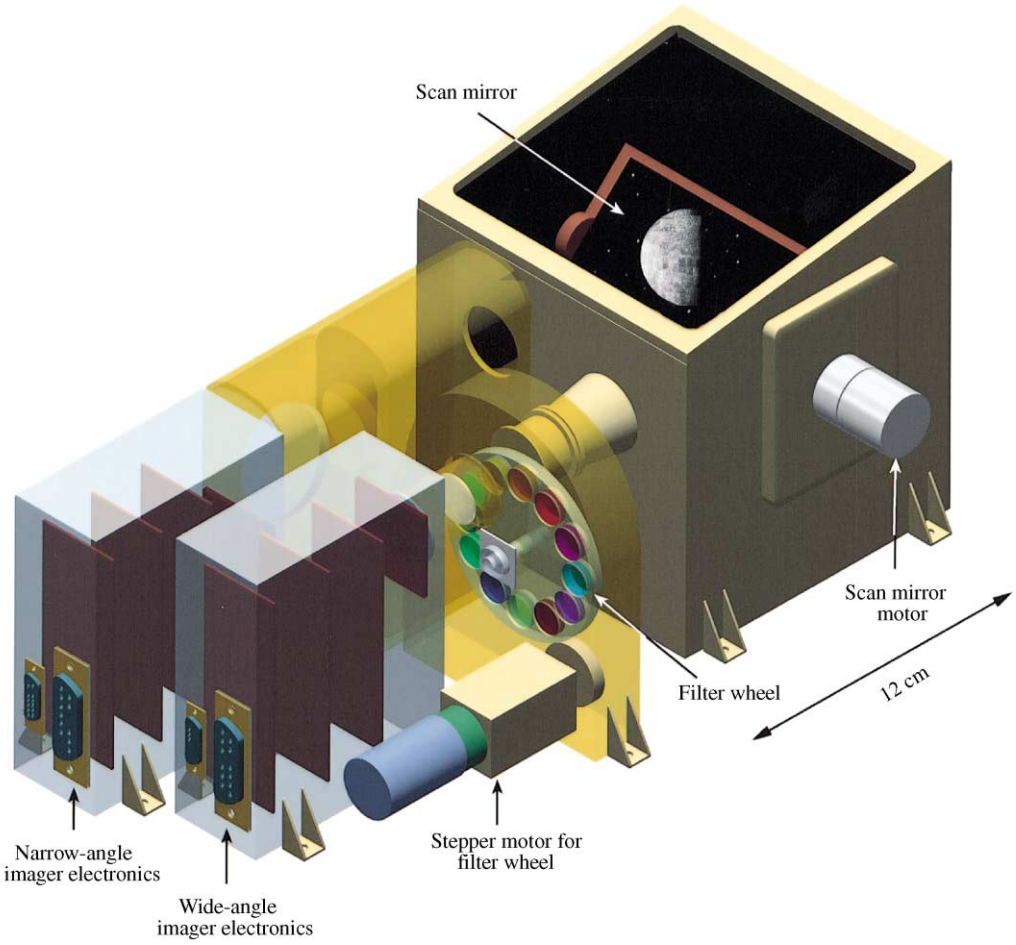

Fig. 1. Mercury Dual Imaging System (MDIS). The opening aperture is to the top and back. The entrance window has been removed to show the scan mirror. The associated stepper motor protrudes to the right through the housing. The optical path of the wide-angle imager intersects the filter wheel. Blue shadowed regions indicate the CCD detectors and associated electronics.

Table 2
MDIS characteristics

	Narrow-angle camera	Wide-angle camera
Scan range	$+50^\circ$ to -20°	
Field-of-view	1.5°	10.5°
Spectral filtering	Single band-limiting filter	12 filter positions
Focal length	550 mm	79 mm
Focal ratio	18	5
Detector	CCD 1024×1024, 14 μm pixels	
Pixel field-of-view	5.2 m at 200 km alt	72 m at 200 km alt
	390 m at 15,000 km	5.4 km at 15,000 km
Signal-to-noise ratio	$> 200:1$	
Quantization	12 bits/pixel	
Compression	Lossless, multi-resolution lossy, 12-to-n bit	
Scan mirror rate	$\geqslant 0.6^\circ\ s^{-1}$	
Scan mirror steps	$\leqslant 0.1^\circ$	

device (CCD) camera heads use highly-integrated, low-mass electronics designed for 12-bit intensity resolution. The WA optics are refractive, and the NA optics are reflective. The two imagers are coaligned. Locating their apertures close to the scan mirror minimizes the size of both the mirror and the heat rejection filter. A thermally isolated baffle reduces stray light and heat from outside the imager field-of-view (FOV).

Spectral information is provided by the WA imager. It has a 10.5° FOV and uses a modified Cooke-triplet lens plus a small field-flattening lens at the CCD detector to assure excellent image quality over the full FOV and wavelength range. Radiation-resistant glasses are used throughout. The lens is achromatic, and the spot size is smaller than the 14 μm pixels over the full field. The optics are inherently small due to the short focal length. The lenses are 30 mm in diameter, and the distance from the first lens surface to the image is only 88 mm. The color filters are chosen to maximize their response to particular ion and mineral spectral features and to give good coverage of the spectral continuum. The 10 color filters are 415 nm center $\times$ 40 wide; 480 $\times$ 30 nm; 560 $\times$ 10 nm; 650 $\times$ 10 nm; 750 $\times$ 10 nm; 830 $\times$ 10 nm; 900 $\times$ 10 nm; 950 $\times$ 20 nm; 1000 $\times$ 30 nm; and 1020 $\times$ 40 nm. The two "clear" filters that are used for optical navigation images are centered at 750 nm, near the peak of the CCD quantum efficiency, and are 600 and 100 nm wide, respectively.

The narrow FOV of 1.5° for the NA imager requires a focal length of 550 mm. A compact, off-axis section of a Ritchey–Chretien reflective telescope is utilized. The mirrors correct spherical aberration and coma. Focal-plane curvature and astigmatism are small, and a correction lens is not required. Performance at 0.4° off axis is diffraction limited, and the spot size is smaller than a pixel over 80% of the FOV. An aperture stop close to the scan mirror minimizes stray light.

Both images use a very-large-scale integrated-circuit (VLSI) chip and a gate array for all clocking, control, and readout of the CCD. Each 1024 × 1024 frame-transfer CCD has manual and automatic exposure control over a range of 1-ms to 10-s exposures with no need of a shutter. On-chip summing of 2 × 2 pixels can be commanded for 512 × 512 images, as required. A hardware subframing capability allows the Science Team to specify that only a chosen rectangular segment of the full image will be saved and transferred to the spacecraft recorder. Both CCDs have thermoelectric coolers for low dark current. Full images can be taken as often as every 4 s, and subframe images may be taken every second, provided that they are no larger than 512 × 512 pixels. Images are transferred directly from the imager to the spacecraft recorder. However, they can be recalled later for processing and compression. Several image-compression techniques are available and may be used individually or in combination. Pixel summing, subframing, and image compression all contribute to the most efficient use of the limited downlink bit rate.

The scan mirror is required for mapping the planet during the flybys and for full-resolution global coverage during the orbital phase of the mission. It is driven by a small stepper motor with redundant windings. (A scan mirror of this design has been under test at JHU/APL continuously stepping in a hard vacuum for more than three years.) The mirror is only 65 mm square and made of light-weight beryllium. The entrance window rejects the infrared thermal radiation from the surface of the planet but transmits the visible and near infrared up to 1100 nm. To ensure that scattered light is not a problem, MDIS will be constructed with low-reflectivity coatings, internal baffles, and a high-quality surface on the heat-rejection filter. Assembly will be done in a class-100 clean room.

Complete calibrations will be conducted at the JHU/APL optical calibration facility and will include measurement of point-spread, geometric distortion, flat field, dark current, radiometric response, wavelength calibration, scattered light, and detector alignment. In-flight calibrations will verify these measurements. MDIS will be turned on for the Venus flybys for flat-field calibration using the Venus disk.

4. Gamma-Ray and Neutron Spectrometer (GRNS)

GRNS has an active-shielded γ-ray scintillator that measures a wide range of elemental abundances (O, Si, S, Fe, H, K, Th, U) and a neutron spectrometer to provide high sensitivity to possible H_2O ice at Mercury's poles. The layout of GRNS is shown in Fig. 2a, and its principal characteristics are listed in Table 3. Like the Near Earth Asteroid Rendezvous (NEAR) Shoemaker γ-ray detector (Trombka et al., 1997), the Gamma-Ray Spectrometer (GRS) scintillator is mounted in a cup-shaped active shield of bismuth germanate (BGO) 1.25 cm thick. The shield defines a ∼ 45° FOV, provides an anticoincidence veto for cosmic rays, protects the central scintillator from locally generated backgrounds, reduces the Compton continuum, and captures escaping γ-rays generated by pair-production in the central scintillator. This design greatly improves the signal-to-background ratio of the γ-ray measurements. NEAR Shoemaker has demonstrated three orders of magnitude background suppression with this type of detector mounted directly to the spacecraft, i.e., without a long, heavy boom (Trombka et al., 1997; Evans et al., 2000).

The primary GRS detector is a 45 × 50 mm^2 cesium iodide (CsI) scintillator directly coupled to a large photodiode. The higher quantum efficiency of the photodiode results in improved γ-ray energy resolution (8.0% vs. 8.7% on NEAR Shoemaker) and eliminates a heavy photomultiplier tube (PMT) that would partially block the entrance aperture. CsI works near room temperature, so cryogenic cooling is not required, and it is nearly immune to radiation damage, important for this long-duration mission. The complex geometry of the GRS shield requires a PMT for light collection; the scintillators and PMT are thermally controlled for gain stability.

The Neutron Spectrometer (NS) subsystem, shown in Fig. 2b and Table 3, uses two paddle-shaped glass scintillators separated by a sheet of neutron absorbing scintillator. The glass scintillators are GS20, which has 6.6% lithium by weight enriched to 95% ^6Li. The difference in counts detected by the GS20 scintillators, when they are oriented in the spacecraft ram and wake directions, gives a measure of the thermal neutron intensity near the planet. The neutron-absorbing scintillator between the two slabs of GS20 counts epithermal and fast neutrons. All scintillators are viewed by separate PMTs.

Ground calibrations will be performed on the GRNS using γ and neutron sources (Evans et al., 2000). In-flight calibration will rely on prominent spectral lines, e.g., the 0.511-MeV annihilation line. Activation will be monitored over time to characterize fully the buildup of the background. The NEAR Shoemaker GRS confirms the efficacy of this approach (Trombka et al., 1997; Evans et al., 2000).

5. X-Ray Spectrometer (XRS)

XRS is an improved version of the NEAR Shoemaker X-ray spectrometer design (Trombka et al., 1997). Three gas proportional counters view the planet, and a state-of-the-art Si-PIN detector mounted on the spacecraft sunshade (Santo

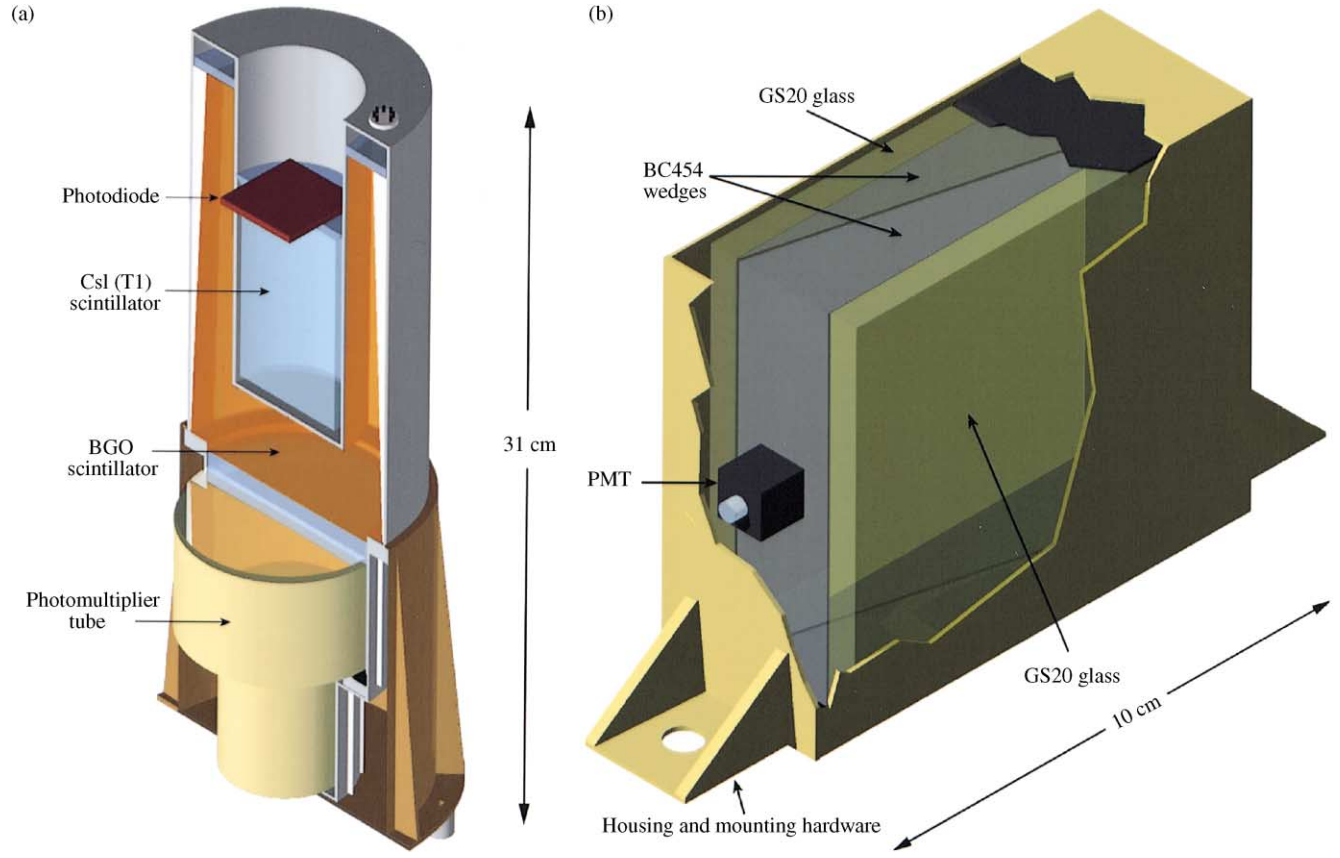

Fig. 2. (a) Gamma-Ray and Neutron Spectrometer (GRNS), Gamma-Ray Spectrometer (GRS) subsystem. This cutaway view of the cylindrically symmetric GRS shows the active BGO shield mounted on top of the associated PMT. The central CsI scintillator is viewed with a solid-state photodiode. (b) GRNS, Neutron Spectrometer (NS) subsystem. The neutron spectrometer detects neutrons from thermal to fast energies. The cutaway view shows two optically isolated wedges of BC454 (borated plastic) sandwiched between sheets of GS20 (^{6}Li-enriched glass). Two PMTs (one of which is shown) view the light output from the plastic wedges that act as a light guide from the Li-glass as well as a moderator for the fast neutrons.

Table 3
GRNS characteristics

GRS	
Measured elements	O, Si, S, Fe, H, K, U, Th
Central detector	CsI(Tl) 45 mm diameter × 50 mm
Resolution	8% full-width half maximum (fwhm) at 662 keV
Readout	Si-PIN diode
Energy range	0.3–10 MeV
Field-of-view	$\sim 45^\circ$
Shield detector	BGO cup, 9.0 cm dia. × 9.5 cm
Energy range	0.1–10 MeV
Resolution	14% fwhm at 662 keV
Escape recovery	60% at 511 keV
Readout	Photomultiplier
Integration period	300 s at periapsis; 1800 s at apoapsis
NS	
Measured quantities	Thermal neutrons in ram and wake; epithermal and fast neutrons
Thermal neutrons	80 cm^2, 6.35 mm thick ^{6}Li scintillator (GS20)
Epithermal and fast neutrons	80 cm^2, plastic scintillator (BC454)
Detector	Photomultiplier
Integration period	300 s at periapsis; 1800 s at apoapsis

et al., 2001) views the Sun (Fig. 3 and Table 4). Thin absorption filters on two of the planet-facing detectors differentially separate the lower energy X-ray lines (Al, Mg, and Si). This balanced filter technique has worked well on NEAR Shoemaker (Trombka et al., 2000). A Be–Cu honeycomb collimator provides a 6° FOV, which is smaller than the planet at apoapsis and eliminates the X-Ray sky background. At intermediate altitudes, spatial resolution improves greatly. The signal-to-noise ratio (SNR) of the planet-facing gas tubes is enhanced by a set of anti-coincidence wires, located near the periphery of the tubes, which catch penetrating cosmic-ray events, and an internal Be liner that blocks X-rays produced by cosmic rays in the detector tube walls. The solar flux monitor, a small (0.1 mm^2) detector that looks through a thin Be foil that provides thermal protection, tracks the solar X-ray input to the planet. Energy spectra are accumulated from 1 to 10 keV, which covers the K-fluorescence emission lines of the elements Mg, Al, Si, S, Ca, Ti, and Fe.

The NEAR Shoemaker mission was the first to fly the high-resolution Si-PIN X-ray detector technology (as a solar flux monitor). An improved version was subsequently flown

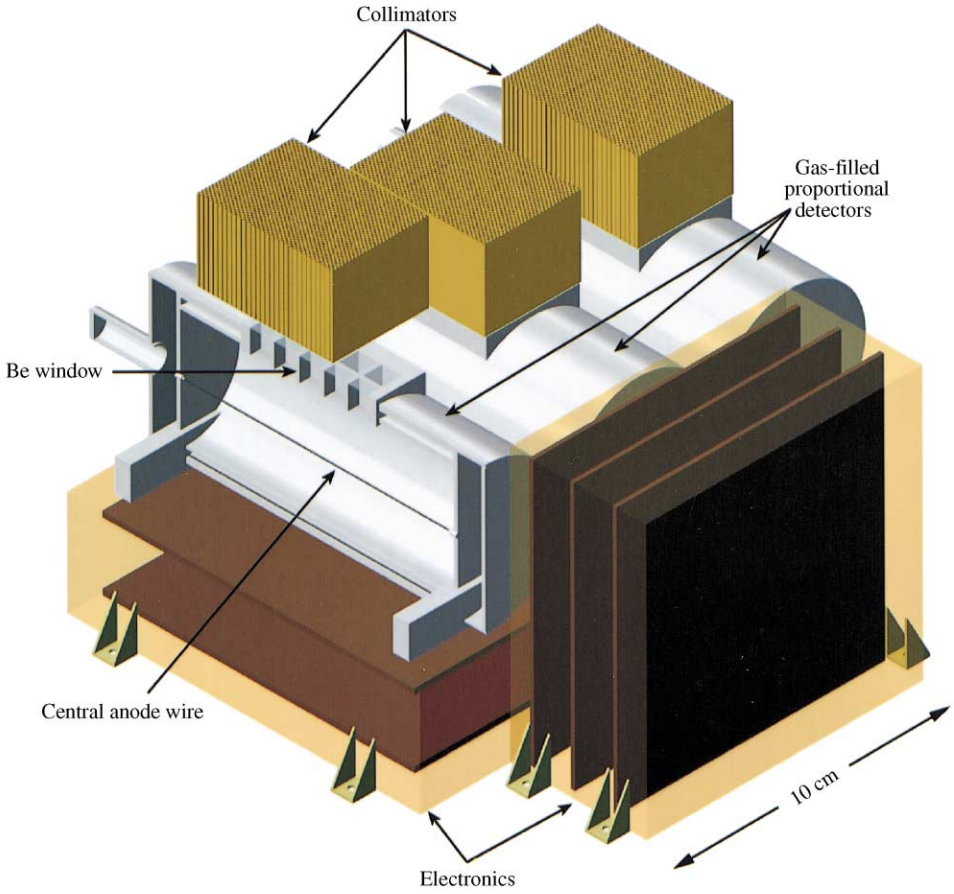

Fig. 3. X-Ray Spectrometer (XRS). The view shows two of the gas-filled proportional counters and their associated collimators in place. One detector has been sectioned and its collimator raised to show the central anode wire. The boxes on the bottom and right front contain the associated electronics.

Table 4
XRS characteristics

Measured elements	Mg, Al, Si, S, Ca, Ti, Fe
Solar monitor	Si-PIN, 300 μm thick, 0.12 mm^2
Detectors	3 gas proportional counters, 10 cm^2 each
Field-of-view	6°, Be–Cu honeycomb collimator
Window	Beryllium 25 μm
Balanced filters	8.5 μm Mg; 8.5 μm Al
Energy range	0.7–10 keV
Energy resolution	350 eV fwhm
Maximum input rate	20 kHz
Integration period	100 s at periapsis; 2000 s at apoapsis

Table 5
MAG characteristics

Detector	3-axis, ring-core fluxgate
Mounting	3.6-m boom
Ranges	±1024 nT, ±65,536 nT
Quantization	16 bits
Internal sample rate	40 Hz
Averaging intervals	0.025–1 s
Readout rates	0.01, 0.1, 1, 10, 20, 40 Hz
AC channel	1–10 Hz

on the Mars Pathfinder rover. The XRS solar flux monitor is a third-generation design that uses discrete resets rather than resistive feedback to compensate for diode leakage currents. This design gives it better energy resolution and greater radiation immunity. Initially, this detector approach was considered for the planet-facing detectors. Experience with the XRS on NEAR Shoemaker (Trombka et al., 2000; Starr et al., 2000), however, has shown that the larger active area available only with the gas tube approach is preferred.

Extensive ground calibrations will be performed on the XRS using both pure elemental samples and assayed samples prepared by the United States Geological Survey. Experience with NEAR Shoemaker shows that no onboard calibration sources are required.

6. Magnetometer (MAG)

MAG is a miniature three-axis, ring-core fluxgate magnetometer with low-noise electronics (Table 5). It is mounted on a 3.6-m boom in the anti-sunward direction. MAG has two ranges with full-scale values of ±1024 and ±65,536 nT. The high range is primarily for ground testing; MAG will operate in the low range in orbit. Field measurements are

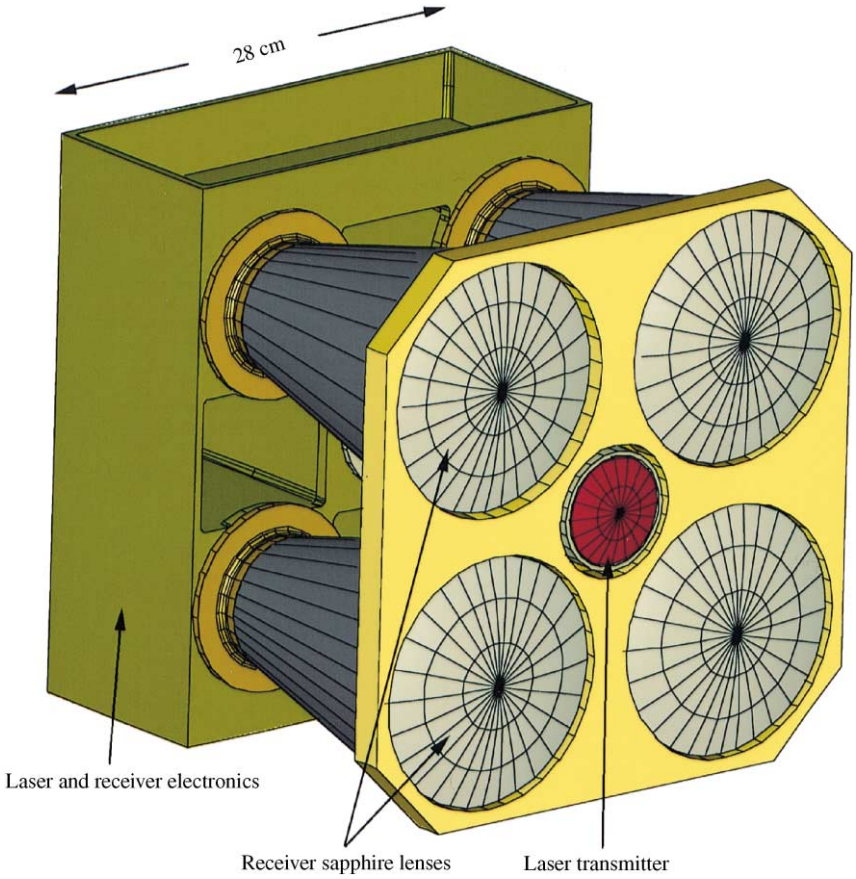

Fig. 4. Mercury Laser Altimeter (MLA). The four sapphire receiver lenses surround the laser transmitter at the center. Electronics are located in the beryllium base structure beneath the laser.

digitized with 16-bit resolution, which provides a minimum quantization of 0.03 nT. The detector samples at a 40-Hz rate. Hardware anti-aliasing filters and digital filtering in the DPU provide selectable averaging intervals from 0.025 to 1 s. At readout rates from 1 to 100 s, a 0.5-s average is provided. Nominal 0.1-Hz sampling of the field will be increased to 10 Hz near periapses and 40 Hz at modeled magnetospheric boundary crossings. Digital filters also provide selectable bandpassed channels of magnetic-field variations. The MAG sensor and processing electronics are almost exact copies of the circuits used in the NEAR Shoemaker design, but the packaging is miniaturized by the use of all surface-mount electronics.

The MAG team is working closely with the spacecraft and other instrument teams to minimize stray spacecraft magnetic fields. Potential magnetic field sources have been identified early in the design process, and mitigation techniques are being selected for their minimum impact on the design. This process worked very well during the development of the Advanced Composition Explorer (ACE). MAG will undergo extensive calibrations at GSFC and JHU/APL prior to integration. Calibrations will be refined in flight. Statistical variance techniques (Davis and Smith, 1968; Belcher, 1973) will be used in the solar wind to determine the spacecraft fields. The same method can be used at the high Mercury-orbit apoapsis.

7. Mercury Laser Altimeter (MLA)

MLA will determine the topography of Mercury in the northern hemisphere where the MESSENGER orbit is less than 1000 km above the surface. The altimeter is based on the instruments flown on Mars Global Surveyor (Zuber et al., 1992; Smith et al., 2001) and the Geoscience Laser Altimeter System (Abshire et al., 1998) to be flown on the Ice, Cloud, and land Elevation Satellite (ICESat). Modifications to the design provide lower mass and longer range while accommodating the thermal loads. MLA consists of a Q-switched, diode-pumped Cr : Nd : YAG laser transmitter operating at 1064 nm, a receiver optical system with four sapphire lenses, a photon-counting detector, a time interval unit (TIU), and processing electronics (Fig. 4 and Table 6).

The laser transmits through a low-mass beam expander with a heat rejection filter at its base and achieves a beam divergence of $\leqslant$ 50 μrad. When the laser fires, a small fraction of the laser beam is sampled by an optical fiber and relayed onto the start detector, which initiates the

Table 6
MLA characteristics

Laser pulse rate	5 Hz
Detection probability	90% at 1000 km range
Spot diameter	10–50 m full width
Spot spacing	100–300 m along track
Ranging precision	0.50 m
Energy resolution	5%, transmit and echo
Laser	Cr : Nd : YAG, passive Q-switched, diode pumped
Wavelength	1064 nm
Pulse	20 mJ, 5 ns fwhm
Beam divergence	$\leqslant$ 50 μrad
Lifetime	$> 5 \times 10^7$ pulses ($>$ 1 year)
Receiver telescope	Four sapphire lenses
Detector	Hybrid avalanche photodiode (photon counting)

timing process in the TIU. The receiver system collects the back-scattered laser echo pulses and passes them through a heat rejection filter and an optical bandpass filter to reject solar background. The pulse is detected with a hybrid avalanche photodiode assembly. Receiver electronics record the arrival time of individually reflected photons. The TIU measures the laser transit time with 50-cm (3.3-ns) range resolution. After detection, the measured width of the echo pulse is used to adjust the estimate of the echo time to approximate the pulse center. This procedure helps correct for pulse dilation from non-nadir pointing and local slopes at the planet. The surface-MLA link margin has been calculated to quantify the transmitted laser energy needed to achieve the required instrument performance based on the expected signal and noise levels. Under worst-case conditions (daytime, 6% surface reflectivity, 5° slopes), MLA has a ranging probability of 90% at a 1000-km slant range. Surface roughness, surface slopes, and spacecraft-pointing effects are the major sources of error in the determination of range.

Pre-flight measurements with a variety of simulated echoes and backgrounds at various distances and return signals will be used to characterize performance.

8. Mercury Atmospheric and Surface Composition Spectrometer (MASCS)

MASCS is derived from the Galileo Ultraviolet Spectrometer (Hord et al., 1992). A well-baffled telescope simultaneously feeds both an UVVS and a VIRS with a common boresight. UVVS is optimized for measuring the composition and structure of the atmosphere and surface reflectance. VIRS is optimized for measuring visible (VIS) and near-infrared (IR) surface reflectance (Table 7). VIRS is mounted on top of the UVVS and is coupled to the telescope focal plane with a short fiber-optic bundle (Fig. 5). Internal electronics manage instrument configuration, control spectral scanning, and provide communications to the DPU. UVVS is very similar to the Galileo Ultraviolet Spectrometer (UVS) with three principal modifications. The aperture and sunshade have been modified to accommodate the Mercury thermal input, the grating is changed for the UVVS wavelength range, and there is a mask at the spectrometer entrance slit. VIRS is a new design. UVVS has 25-km resolution at the limb; VIRS has 100-m to 7.5-km resolution on the surface of Mercury, depending on altitude.

Table 7
MASCS characteristics

	UVVS	VIRS
Telescope	250 mm, $f/5$	
Focal length	125 mm	210 mm
Spatial resolution	25 km on limb	100 m–7.5 km
Grating	1800 lines/mm	120 lines/mm
Spectral resolution	0.5 nm FUV	
	1.0 nm MUV, VIS	4 nm
Wavelength range	FUV 115–190 nm	VIS 0.300–1.025 μm
	MUV 160–320 nm	IR 0.95–1.45 μm
	VIS 250–600 nm	
Detector	3 PMT: CsI, CsTe, Bi-Alkali	512 × 1, Si,
		256 × 1, InGaAs
FOV	$1^\circ \times 0.05^\circ$ atmosphere	$0.023^\circ \times 0.023^\circ$
	$0.023^\circ \times 0.023^\circ$ surface	
Sensitivity	10 R in 100 s (5σ)	SNR $>$ 200

MASCS has a Cassegrain telescope that feeds an Ebert–Fastie diffraction grating spectrometer in the UVVS. The thermally isolated external light shade and the extensive baffle system reject stray light; the Galileo UVS has demonstrated off-axis scattered light rejection greater than 10^5 for point sources $\geqslant 1^\circ$ from the FOV (Hord et al., 1992).

An 1800-groove/mm grating provides an average spectral resolution of 1.0 nm. The spectrum is scanned by rotating the grating in 0.25 nm steps, providing a factor of 4 oversampling. Three small PMTs, behind separate slits, are used in pulse-counting mode for the atmospheric observations where high sensitivity is required. The PMTs cover the Far Ultraviolet (FUV), Middle Ultraviolet (MUV), and Visible (VIS). Both FUV and MUV may also be used for surface reflectance measurements. The VIS detector is protected from damage by a limb sensor that disables its high voltage before the FOV intercepts the sunlit disk of the planet. UVVS is optimized to observe weak atmospheric emission from both atoms and molecules. Expected atmospheric limb emission rates range from 10 Rayleighs (R) to a few kR. Over the range 0.19–0.45 μm, 100-s integration times give a SNR of 10 for emissions as weak as 10 R.

A mature, scanning spectrometer design is most appropriate for measuring exospheric emissions on MESSENGER, which requires low mass, moderate resolution, and very high sensitivity for a small number (10–20) of isolated emission lines at known wavelengths spaced within a very broad wavelength range (0.115–0.60 μm). UVVS will give greater sensitivity and resolution for the widely separated weak lines than a spectrograph built around a line-array detector. Observing a few weak lines requires a low-noise detector to build up the signal-to-noise ratio over the relatively long observing times. A photomultiplier tube

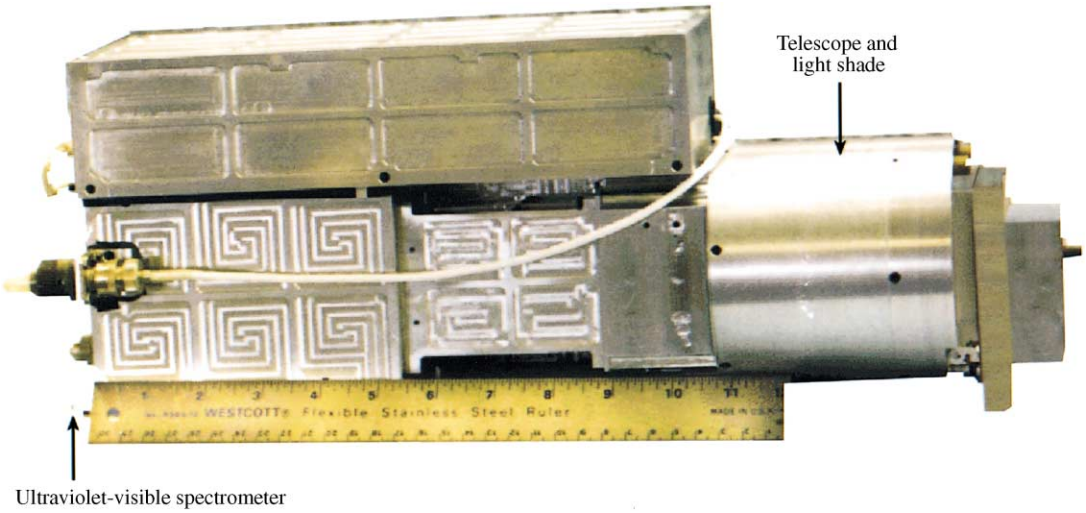

Fig. 5. Mercury Atmospheric and Surface Composition Spectrometer (MASCS). The engineering model of the Galileo Ultraviolet Spectrometer (UVS) shown here is very similar to MASCS.

detector is much better suited to this type of observation than a semiconductor line array. Despite its somewhat lower quantum efficiency, the PMT is a nearly noiseless device, and UVVS will develop an SNR greater than 100 in 1 s for most of the expected emission lines. The wide separation of the lines also means that a line-array detector would require a very large number of pixels, most of which would have no signal, or it would have limited spectral resolution. There is ample time in the orbital phase to make a thorough search for unsuspected emissions over the entire spectral range.

VIRS is designed to measure surface reflectance (0.3–1.45 μm). Light is fed to VIRS through a fused-silica fiber-optic bundle. A concave holographic diffraction grating images onto two semiconductor detectors. A dichroic beam splitter separates the visible (300–1025 nm) and infrared (0.95–1.45 μm) spectra. The visible detector is a 512-element silicon line array which has an absorption filter in front of the long-wavelength half to eliminate the second-order spectrum (Maymon et al., 1988). The IR detector is a 256-element InGaAs array, which does not require cooling. Both detectors are digitized to 12 bits. A 1-s integration will provide SNR $>$ 200. The 1.45-μm long-wavelength cutoff for VIRS was chosen because thermal emission from Mercury's surface beyond that wavelength is comparable to the reflected solar signal.

In addition to standard laboratory calibrations, UVVS and VIRS will be active during the two Venus flybys to acquire spectra that can be compared with previous Venus spectral results.

9. Energetic Particle and Plasma Spectrometer (EPPS)

EPPS measures ions from thermal plasmas through $\sim$5 MeV and electrons from $\sim$ 20 to 700 keV. EPPS combines a FIPS head for thermal plasmas and an EPS head for energetic ions and electrons, with central electronics in a compact and low-mass instrument (Fig. 6 and Table 8). EPPS is mounted on the side of the spacecraft, near the top deck, and close to the edge of the shadow from the sunshade (Santo et al., 2001), where it can observe low-energy ions coming up from the surface of Mercury, pickup ions, ions and electrons accelerated in the magnetosphere, and the solar wind when the spacecraft is turned near its maximum allowed off-Sun pointing angle (Santo et al., 2001). This mounting also minimizes the thermal input from the planet onto the EPS entrance foil. Both EPS and FIPS use a time-of-flight (TOF) system to determine the velocity (energy/mass) of the detected ions.

EPS is a hockey-puck-sized, TOF spectrometer that measures the energy spectra, atomic composition, and pitch-angle distributions of energetic ions from 10 keV/nuc to $\sim$ 5 MeV and electrons from $\sim$ 20 to 700 keV. EPS measures the ion TOF using secondary electrons generated as the ion passes through the entrance and exit foils in the spectrometer. Total energy is measured by a pixelated silicon detector. A collimator defines the acceptance angles for the six pixel segments. The FOV is 160° by 12° with six active segments of 25° each; the geometric factor is $\sim$ 0.1 cm^2 sr. The "start" and "stop" signals for the TOF measurements (up to 200 ns) are detected by a micro-channel plate (MCP) electron multiplier. Timing, energy, and event-classification chips produce an eight-point energy spectrum for each of four species in all six pixel directions. Spectra are read out, on average, every 36 s. Electrons are measured in two of the 25° segments. These pixels have both a bare silicon detector and a foil-covered detector to provide electron-ion separation. An engineering model of EPS has operated well at the accelerator facility at GSFC.

EPS will be fully calibrated using α-particle and accelerator sources prior to integration with the spacecraft. Flight experience with similar instrumentation built by JHU/APL

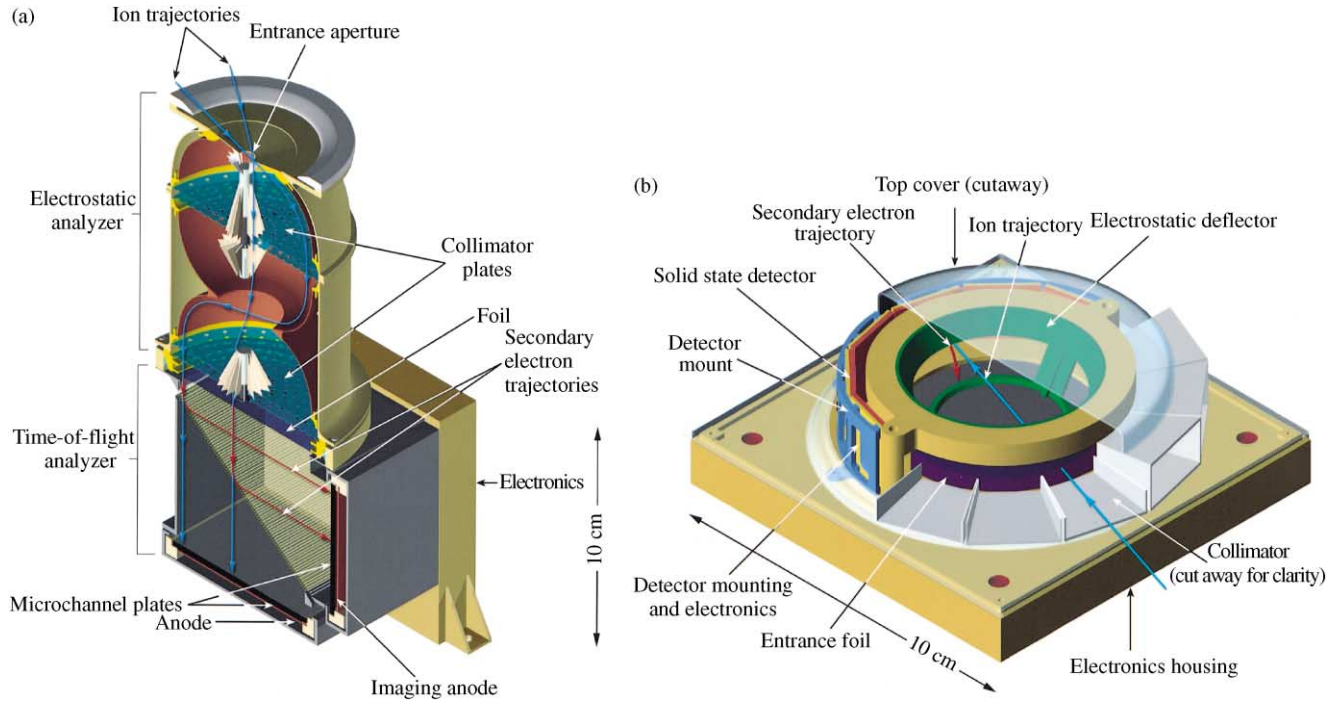

Fig. 6. Energetic Particle and Plasma Spectrometer (EPPS). (a) The electrostatic analyzer behind the FIPS entrance aperture accepts particles over most of the exposed hemisphere. The elevation and azimuth angles of particles entering the analyzer with the selected energy-per-charge are mapped onto the radius and azimuth of the thin foil at the electrostatic analyzer exit. The position and velocity of these particles are measured in the time-of-flight analyzer at the base of the FIPS head. (b) Energetic ions entering through the EPS collimator pass through entrance and exit foils before stopping in a silicon solid-state detector. Secondary electrons released at the foils provide start and stop signals to determine the particle velocity, and the solid-state detector measures the particle total energy. The six solid-state detector assemblies determine particle direction.

Table 8
EPPS characteristics

FIPS	
Measured species	H, ^{3}He, ^{4}He, O, Ne, Na, K, S, Ar, Fe
Field-of-view	360° azimuth × 70° elevation
Geometrical factor	$\sim$ 0.05 cm^2 sr
Entrance foil	$\sim$ 1.0 μg/cm^2 carbon
TOF range	50 ns–500 ns
Deflection voltage	0.0–8.0 kV
Energy/charge range	0.0–10.0 keV/q
Voltage scan period	1 min
EPS	
Measured species	H, He, CNO, Fe, electrons
Field-of-view	160° × 12°
Geometrical factor	$\sim$ 0.1 cm^2 sr
Foils	Aluminized polyimide; 9 μg/cm^2
TOF range	0–200 ns, ±200 ps (1 σ)
Peak input rate	1 MHz
Detectors	6 Si, 500-μm thickness, 2 cm^2 each
Energy range	10 keV/nuc–5 MeV total energy
Integration period	Variable, 36 s average

for Voyager (Krimigis et al., 1977), Active Magnetospheric Particle Tracer Explorers (AMPTE) (McEntire et al., 1985), Galileo (Williams et al., 1992), Geotail (Williams et al., 1994), ACE (Gold et al., 1998), and Cassini (Mitchell et al., 1998) shows that the tracks of energy vs. time of flight are well separated and are therefore self-calibrating for atomic species, so that no in-flight calibration source is required.

FIPS measures low-energy plasmas in the Mercury environment in a range of energy per charge (E/q) from a few eV/q (determined by the spacecraft potential) up to $\sim$ 10 keV/q. FIPS has nearly full hemispherical coverage with its electrostatic analyzer (Zurbuchen et al., 1998). Particles of the correct E/q and polar angle pass through the dome-shaped electrostatic deflection system and into a position-sensing TOF telescope. For a given polar incidence angle, a setting of the deflection voltage allows only ions within a narrow E/q range to pass through the deflection system. The ions are then post-accelerated by a fixed voltage before passing through a very thin ($\sim$ 1 μg/cm^2) carbon foil. The ions travel a known distance and hit the stop MCP assembly, while the forward-scattered electrons from the carbon foil are focused onto the start MCP. Position sensing of the start electrons with a wedge-and-strip anode in the MCP assembly determines the initial incidence angle. The mass per charge of a given ion follows from E/q and the TOF, allowing reconstruction of distribution functions for different mass/charge species. The deflection voltage is stepped from 0 to 8 kV over 1 min and covers an E/q range of $\sim$ 0.0 to $\sim$10.0 keV/q. A prototype of the electrostatic analyzer has been successfully tested in the accelerator facility at GSFC.

Table 9
MESSENGER payload resource requirements

Instrument	Volume (cm^3)	FOV	Interface temperature (survival/in-calibration, °C)	Alignment/ pointing control/ knowledge	Daily data volume (Mb/d)	Contamination requirements
MDIS	$27 \times 26 \times 12$ + baffle	NA-1.5° WA-10.5°	−34 +65/ −30 +25	0.1°/0.1°/0.02°	32.9	N_2 purge
GRNS GRS NS	$22.2 \times 15 \times 15$ $10 \times 10 \times 10$	80°, 2π	−34 + 65/ − 20 + 35	1°/2°/1°	10.6	—
XRS	$8.6 \times 8.6 \times 10.6$	6°	−34 + 65/ − 30 + 35	1°/1°/0.1°	4.2	—
MAG	$3 \times 2 \times 2$ $10 \times 10 \times 4$	4π sr	−90 + 180/ −90 + 180	1°/1°/1°	1.2	Field < 1.0 nT at MAG
MLA	$28 \times 28 \times 26$	150 μrad	isolated	0.1°/0.1°/0.03°	4.0	N_2 purge
MASCS	$34 \times 19 \times 12$	1.0° × 0.05°	−34 + 55/ − 20 + 40	0.1°/0.1°/0.05°	7.5	N_2 purge
EPPS	$19 \times 13 \times 14$	160° × 12°, 360° × 75°	−34 + 60/ − 20 + 35	1°/1°/1°	12.1	N_2 purge
DPU + instrument power	$18 \times 11 \times 11$ $15 \times 15 \times 7.5$	N/A	−34 + 65/ − 29 + 30	N/A	0.9	—

The EPPS common electronics process all of the TOF, energy, and position signals from the MCPs and the solid-state detectors. TOF is measured by a custom application-specific integrated circuit which can provide ±50 ps timing resolution for only 30 mW of power (Paschalidis et al., 1998). Also included in the common electronics are the MCP high-voltage supplies and the FIPS electrostatic deflection high-voltage supply.

10. Radio Science (RS)

Radio science observations are required for measurements of Mercury's gravity field and in support of the laser altimetry investigation. In particular, accurate knowledge of spacecraft location is required to recover the magnitude of the physical libration of the planet, a key mission objective (Solomon et al., 2001). Tracking (range-rate measurement) of the MESSENGER spacecraft relative to the Earth is required to 0.1 mm/s root-mean-square (rms) error $(1-\sigma)$ over a 60-s integration period; the corresponding laser altimetry requirement is 1 m rms $(1-\sigma)$ to the surface of Mercury. The performance requirements are met by the telecommunications subsystem and Deep Space Network (DSN) with standard operations at existing facilities.

11. Data processing unit (DPU)

The DPU provides all of the instrument processing, high-level electronics, and power converters or power switching. Dual RTX2010 processors are fully redundant and cross-strapped. No single-point failure will disable the instrument suite. Each processor has 256 kB of RAM, 256 kB of EEPROM and 64 kB of ROM memory. The DPU core is flying on the Cassini Magnetospheric Imaging Instrument (MIMI) (Mitchell et al., 1998). Instrument-specific interface cards connect the payload to the DPU core. Processor and bus margins are sufficient to allow full instrument operation with any single redundant-component failure. The software for MDIS, GRNS, XRS, MAG, and EPPS are nearly identical to the existing software from similar instruments flown or currently flying on Cassini, ACE, and NEAR Shoemaker. MLA and MASCS software, while new, requires only simple serial data collection and command passing.

12. Payload resource requirements

A payload places resource requirements on the spacecraft beyond the mass and power listed in Table 1. The spacecraft must accommodate the instrument volume, FOV, and other requirements. A summary of the MESSENGER payload resource requirements is given in Table 9. Most of the instruments are mounted on the lower deck of the spacecraft, primarily inside the adapter to the launch vehicle third stage (Fig. 7). Only the MAG is boom mounted. The directional instruments are co-aligned so that they all view the same portion of Mercury simultaneously. Pointing is accomplished by spacecraft pitch and yaw to keep the spacecraft lower deck aimed at Mercury (Santo et al., 2001). Pointing maneuvers are limited by the maximum allowable off-Sun-pointing

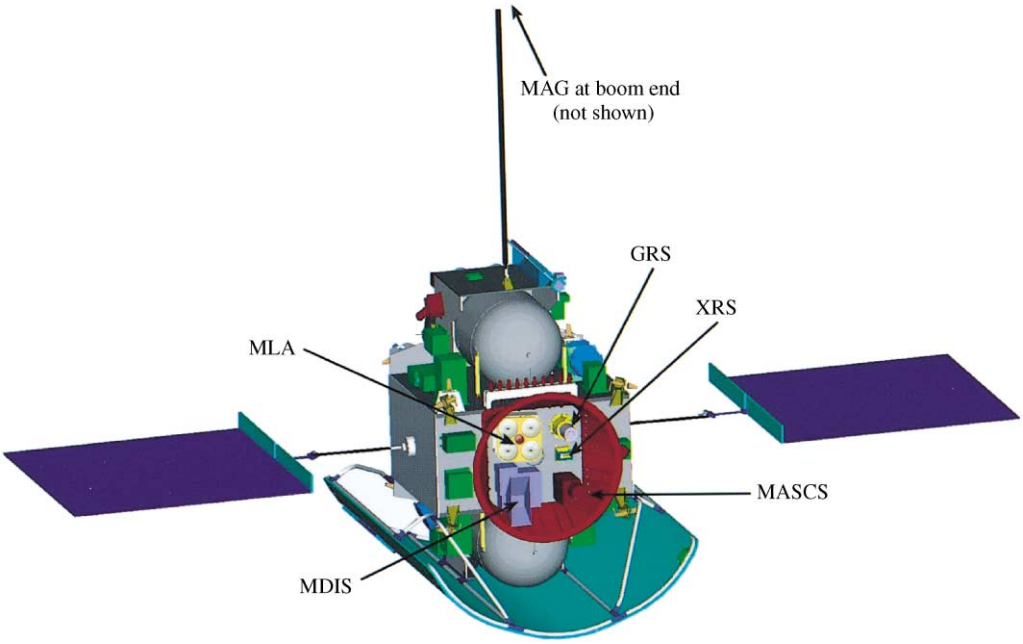

Fig. 7. MESSENGER spacecraft showing instrument placement.

of the spacecraft sunshade. Therefore, there are small intervals when MESSENGER is in a nearly noon-midnight orbit around Mercury when the off-Sun-pointing limits prevent the instruments from viewing the planet; these constraints are taken into account in the mission-operation plans (Solomon et al., 2001).

The experience of the NEAR Shoemaker mission, with a similar attitude control system, predicts that the actual pointing accuracy and knowledge will be significantly better than the requirements. Most of the fields of view are clear; however, the solar panels may partially obstruct the nearly full-hemisphere FOV of the EPPS FIPS head for some panel rotation angles. The GRNS NS head is mounted so that it is shielded by approximately the same spacecraft mass when it is aligned with the orbital ram and wake directions. To meet the thermal requirements for each instrument, some are isolated from the spacecraft structure while others are tied to it.

Because there are three optical instruments on MESSENGER, contamination will be carefully controlled. In addition, the optical instruments and EPPS will be purged with N_2 during ground operations. Magnetic contamination will also be carefully controlled to ensure that the MAG will be able to map accurately the internal magnetic field of Mercury as well as its interactions with the solar wind.

13. Conclusion

The MESSENGER mission to Mercury, to be completed during the current decade, will provide important new insight into the formation and early history of the inner planets. This mission, carried out under the National Aeronautics and Space Administration's Discovery Program, is subject to both launch-vehicle and financial constraints. These constraints along with the unusual thermal environment of Mercury and the scientific imperative to orbit the planet, drive the spacecraft design (Santo et al., 2001) and operational characteristics (Solomon et al., 2001). The seven instruments on the MESSENGER spacecraft are integrated with the spacecraft and mission design using a systems optimization approach that, combined with an aggressive miniaturization program, allow all scientific measurement requirements for the mission to be met in full.

Acknowledgements

We thank Barbara Northrop for assistance with manuscript preparation. The MESSENGER mission is supported by the NASA Discovery Program under contracts to the Carnegie Institution of Washington (NASW-00002) and The Johns Hopkins University Applied Physics Laboratory (NAS5-97271).

References

Abshire, J.B., Smith, J.C., Schutz, B.E., 1998. The Geoscience Laser Altimeter System. Technical Digest, 19th International Laser Radar Conference. Annapolis, MD, NASA Conference Report CP-1998-207671, pp. 211–214.

Belcher, J.W., 1973. A variation of the Davis–Smith method for in-flight determination of spacecraft magnetic fields. J. Geophys. Res. 78, 6480–6490.

Chapman, C.R., 1988. Mercury: introduction to an end-member planet. In: Vilas, F., Chapman, C.R., Matthews, M.S. (Eds.), Mercury. University of Arizona Press, Tucson, pp. 1–23.

Davis Jr., L., Smith, E.J., 1968. The in-flight determination of spacecraft field zeroes. Eos Trans. Am. Geophys. Union 49, 257.

Dunne, J.A., Burgess, E., 1978. The Voyage of Mariner 10: Mission to Venus and Mercury. NASA SP-424. NASA Scientific and Technical Information Office, Washington, DC, 124pp.

Evans, L.G., Starr, R., Trombka, J.I., McClanahan, T.P., Bailey, S.H., Mikheeva, I., Bhangoo, J.J., Brückner, J., Goldsten, J.O., 2000. Calibration of the NEAR gamma-ray spectrometer. Icarus 148, 95–117.

Gold, R.E., Krimigis, S.M., Hawkins, S.E., Haggerty, D.K., Lohr, D.A., Fiore, E., Armstrong, T.P., Holland, G., Lanzerotti, L.J., 1998. Electron, proton and alpha monitor on the Advanced Composition Explorer spacecraft. Space Sci. Rev. 86, 541–562.

Hord, C.W., McClintock, W.E., Barth, C.A., Esposito, L.W., Stewart, A.I.F., Thomas, G.E., Sandel, B.R., Hunten, D.M., Broadfoot, A.L., Shemansky, D.E., Ajello, J.M., Lane, A.L., West, R.W., 1992. Galileo Ultraviolet Spectrometer experiment. Space Sci. Rev. 60, 503–530.

Krimigis, S.M., Armstrong, T.P., Axford, W.I., Bostrom, C.O., Fan, C.Y., Gloeckler, G., Lanzerotti, L.J., 1977. The Low Energy Charged Particle (LECP) experiment on the Voyager spacecraft. Space Sci. Rev. 21, 329–354.

Maymon, S.W., Neeck, S.P., Moody Sr. J.C., 1988. Optical design alternatives for the Moderate-resolution Imaging Spectrometer for the earth orbiting system. Soc. Photo-Opt. Instrum. Eng. 924, 10–22.

McEntire, R.W., Keath, E.P., Fort, D.E., Lui, A.T.Y., Krimigis, S.M., 1985. The Medium-Energy Particle Analyzer (MEPA) on the AMPTE CCE spacecraft. IEEE Trans. Geosci. Remote Sensing GE-23, 230–233.

Mitchell, D.G., Krimigis, S.M., Cheng, A.F., Jaskulek, S.E., Keath, E.P., Mauk, B.H., McEntire, R.W., Roelof, E.C., Schlemm, C.E., Tossman, B.E., Williams, D.J., 1998. The imaging neutral camera for the Cassini mission to Saturn and Titan. In: Pfaff, R.F., Borovsky, J.E., Young, D.T. (Eds.), Measurement Techniques in Space Plasmas: Fields, AGU Geophysical Monograph, Vol. 103. American Geophysical Union, Washington, DC, pp. 281–287.

Paschalidis, N., Karadamoglou, K., Stamatopoulos, N., Paschalidis, V., Kottaras, G., Sarris, E., Keath, E., McEntire, R., 1998. An integrated time to digital converter for space instrumentation. In Seventh NASA Symposium on VLSI Design. University of New Mexico, Albuquerque, NM, pp. 5.4.1–5.4.8.

Santo, A.G., Gold, R.E., McNutt Jr., R.L., Solomon, S.C., Ercol, C.J., Farquhar, R.W., Hartka, T.J., Jenkins, J.E., McAdams, J.V., Mosher, L.E., Persons, D.F., Artis, D.A., Bokulic, R.S., Conde, R.F., Dakermanji, G., Goss Jr., M.E., Haley, D.R., Heeres, K.J., Maurer, R.H., Moore, R.C., Rodberg, E.H., Stern, T.G., Wiley, S.R., Williams, B.G., Yen, C.L., Peterson, M.R., 2001. The MESSENGER mission to Mercury: spacecraft and mission design. Planet. Space Sci., this issue.

Smith, D.E., Zuber, M.T., Frey, H.V., Garvin, J.B., Head, J.W., Muhleman, D.O., Pettengill, G.H., Phillips, R.J., Solomon, S.C., Zwally, H.J., Banerdt, W.B., Duxbury, T.C., Golombek, M.P., Lemoine, F.G., Neumann, G.A., Rowlands, D.D., Aharonson, O., Ford, P.G., Ivanov, A.B., McGovern, P.J., Abshire, J.B., Afzal, R.S., Sun, X., 2001. Mars orbiter laser altimeter (MOLA): experiment summary after the first year of global mapping of Mars. J. Geophys. Res., in press.

Solomon, S.C., McNutt Jr., R.L., Gold, R.E., Acuña, M.H., Baker, D.N., Boynton, W.V., Chapman, C.R., Cheng, A.F., Gloeckler, G., Head III, J.W., Krimigis, S.M., McClintock, W.E., Murchie, S.L., Peale, S.J., Phillips, R.J., Robinson, M.S., Slavin, J.A., Smith, D.E., Strom, R.G., Trombka, J.I., Zuber, M.T., 2001. The MESSENGER mission to Mercury: scientific objectives and implementation. Planet. Space Sci., this issue.

Starr, R., Clark, P.E., Murphy, M.E., Floyd, S.R., McClanahan, T.P., Nittler, L.R., Trombka, J.I., Evans, L.G., Boynton, W.V., Bailey, S.H., Bhangoo, J., Mikheeva, I., Brückner, J., Squyres, S.W., McCartney, E.M., Goldsten, J.O., McNutt Jr., R.L., 2000. Instrument calibrations and data analysis procedures for the NEAR X-ray spectrometer. Icarus 148, 498–519.

Trombka, J.I., Floyd, S.R., Boynton, W.V., Bailey, S., Brückner, J., Squyres, S.W., Evans, L.G., Clark, P.E., Starr, R., Fiore, E., Gold, R., Goldsten, J., McNutt, R., 1997. The NEAR X-ray/gamma-ray spectrometer. J. Geophys. Res. 102, 23,729–23,750.

Trombka, J.I., Squyres, S.W., Brückner, J., Boynton, W.V., Reedy, R.C., McCoy, T.J., Gorenstein, P., Evans, L.G., Arnold, J.R., Starr, R.D., Nittler, L.R., Murphy, M.E., Mikheeva, I., McNutt Jr., R.L., McClanahan, T.P., McCartney, E., Goldsten, J.O., Gold, R.E., Floyd, S.R., Clark, P.E., Burbine, T.H., Bhangoo, J.S., Bailey, S.H., Petaev, M., 2000. The elemental composition of asteroid 433 Eros: results of the NEAR-Shoemaker X-ray spectrometer. Science 289, 2101–2105.

Williams, D.J., McEntire, R.W., Jaskulek, S., Wilken, B., 1992. The Galileo Energetic Particle Detector. Space Sci. Rev. 60, 385–412.

Williams, D.J., McEntire, R.W., Schlemm II, C., Lui, A.T.Y., Gloeckler, G., Christon, S.P., Gliem, F., 1994. Geotail energetic particles and ion composition instrument. J. Geomag. Geoelectr. 46, 39–57.

Zuber, M.T., Smith, D.E., Solomon, S.C., Muhleman, D.O., Head, J.W., Garvin, J.B., Abshire, J.B., Bufton, J.L., 1992. The Mars Observer Laser Altimeter investigation. J. Geophys. Res. 97, 7781–7798.

Zurbuchen, T.H., Gloeckler, G., Cain, J.C., Lasley, S.E., Shanks, W., 1998. Low-weight plasma instrument to be used in the inner heliosphere. In: Korendkye, C.M. (Ed.), Missions to the Sun II, Proc. Soc. Photo-Opt. Instrum. Eng. 3442, 217–224.